Supplementary materials

The development of a method to produce diagnostic reagents using $LaNiO_3$ nanospheres and their application in nanozyme-linked immunosorbent assay for the colorimetric screening of C-reactive protein with high sensitivity

Maria Nikitina*[a,b], Pavel Khramtsov[a,b], Stepan Devyatov[b], Rishat Valeev[c], Marina Eremina,[c], Andrey Chukavin,[c] and Mikhail Rayev[a,b]

[a] Institute of Ecology and Genetics of Microorganisms, Urals branch of RAS, Perm, Russia.

[b] Biology faculty, Perm State University, Perm, Russia

[c] Udmurt Federal Research Center, Ural Branch of RAS, Izhevsk, Russia.

*Corresponding author.
E-mail addresses:
kropanevamasha@gmail.com
(M. Nikitina)

Materials

Tween-20, glutaraldehyde, citric acid, glycine, sodium phosphate, sodium bicarbonate, and glycerol were from ITW (USA). Citric acid and MES was from Helicon (Russia). Mouse monoclonal IgG2a against human CRP (clone C2 and C6cc) further designated as C2 and C6cc, recombinant human CRP, procalcitonin (PCT), Serum amyloid A1 and A2 (SAA1 and SAA2), and canine CRP (CRPc) were obtained from HyTest (Finland). Human serum amyloid P component (SAP) was from CusaBio (China). Casein, 11.77 M hydrogen peroxide were from Sigma-Aldrich (USA). Bovine serum albumin was from Biosera (France). 3,3',5,5'-tetramethylbenzidine dihydrochloride (TMB) and HEPES were from AppliChem (USA). Sulphuric acid and hydrochloric acid were from Reakhim (Russia). Standard PBS tablets (10 mM sodium phosphates + 0.137 M NaCl + 0.0027 M KCl, pH 7.4) were from Ecoservice (Russia). Sodium hydroxide, Na_2-EDTA were from Dia-M (Russia). Lanthanum (III) nitrate, nickel (II) nitrate were from Chemcraft (Russia).

Instrumentation

Multiskan Sky UV-Vis Reader was from Thermo Scientific (USA). ZetaSizer NanoZS particle analyzer was from Malvern (UK). VCX-130 ultrasonic processor was from Sonics & Materials (USA).

Polystyrene ELISA plates with high protein binding were obtained from Kirgen (China).

Buffer for the preparation of LNNP's conjugates: HEPES solution was adjusted to pH 7 with 1 M HCl

Buffers for NLISA:

Coating buffer: 0.2 M sodium carbonate bicarbonate buffer, pH 9.6;

Washing buffer: PBS + 0.1% Tween-20 (PBST).

Substrate buffer: 20 mmol/L of HEPES, 20 mmol/L of MES, 20 mmol/L of sodium acetate, 100 mmol/L of NaCl; pH was adjusted with 5 mol/L NaOH or 5 mol/L HCl.

Substrate solution: 0.55 mL of 4 mg/mL of TMB in DMSO; 9.482 mL of substrate buffer; 0.748 mL of 11.77 M H_2O_2; 0.22 mL of 0.1 mmol/L Na_2-EDTA.

All buffers were prepared using deionized water.

Characterization of $LaNiO_3$@BSA/C6cc.

The size (Z-average, nm) and monodispersity of nanoparticles were measured by dynamic light scattering (DLS). For this, nanoparticles were diluted with deionized water 1:125.

To assess the absorbance at 450 nm of the $LaNiO_3$@BSA/C6cc obtained suspensions were diluted 1:20 in the deionized water+1%BSA+20% glycerol

Concentration of unmodified $LaNiO_3$ nanospheres in suspensions was determined by the gravimetric analysis. One milliliter of suspension was added to the porcelain crucibles and dried to constant weight at +115 °C. Mean of three technical replicates was calculated.

SEM images were obtained using Merlin (Carl Zeiss, Germany) and Hitachi HT7700 Excellence (Hitachi, Japan).

XPS spectra were recorded on X-Ray Photoelectron Spectrometer SPECS (Germany) using Mg K-α excitation (E_{ex}= 1253.64 eV). All spectra were calibrated on C sp2 line (E_b=284.6 eV). XPS data were processed applying the CasaXPS software package. Deconvolution was performed using Shirley type background and Gauss (50%)-Lorents (50%) functions. FWHM for all spectra components for each component of chemical elements (Ni, La) were fixed [1], [2].

X-ray diffraction (XRD) was conducted on a Rigaku Miniflex 600 diffractometer with Co Kα radiation (λ = 1.78897 Å) and the diffraction angle 2θ ranged from 10 to 130° with the step 0.02°. Full-profile fitting of the diffraction pattern was performed using the Rietveld method using FullProf Suite programs. X-ray diffraction (XRD) was conducted on a Rigaku Miniflex 600 diffractometer with Co Kα radiation (λ = 1.78897 Å) and the diffraction angle 2θ ranged from 10 to 130° with the step 0.02°. Full-profile fitting of the diffraction pattern was performed using the Rietveld method using FullProf Suite programs [1].

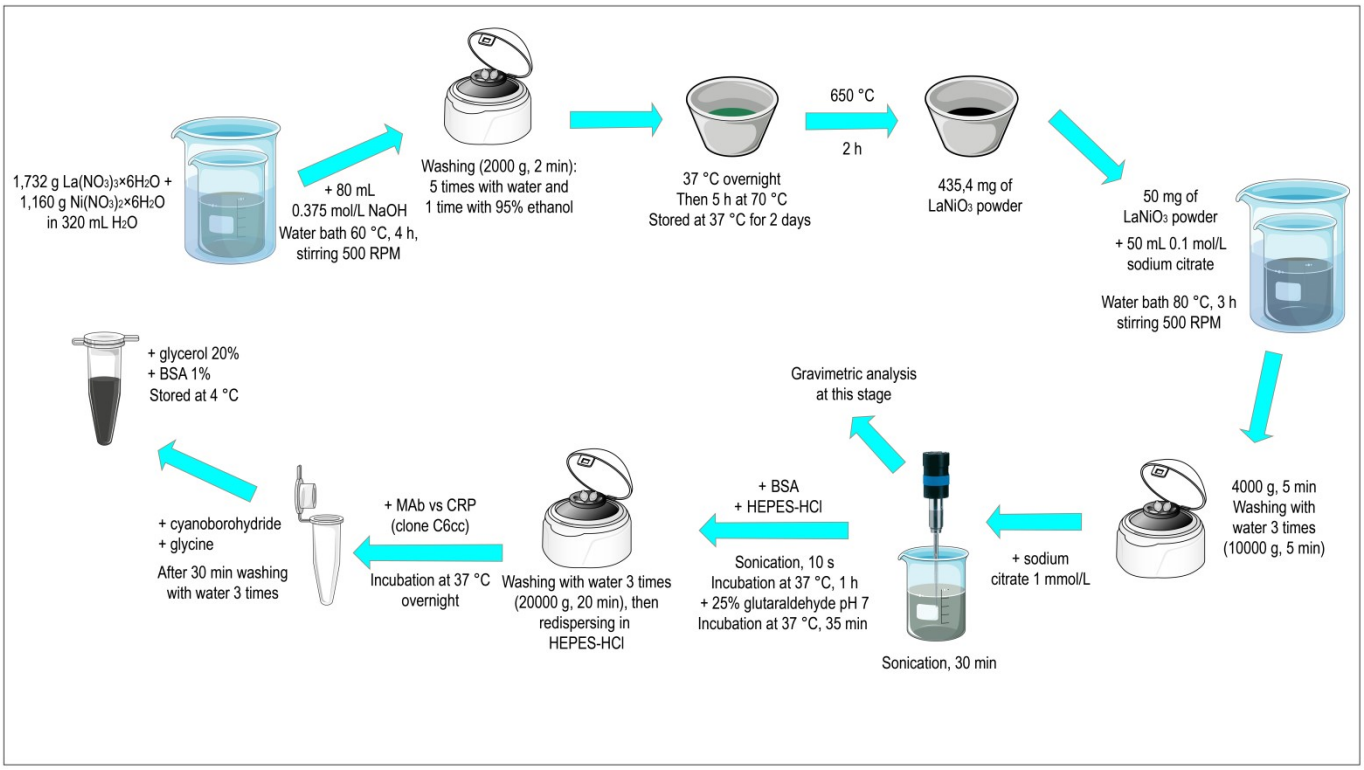

Fig. S1. Scheme of $LaNiO_3$ nanospheres production and modification with Mab.

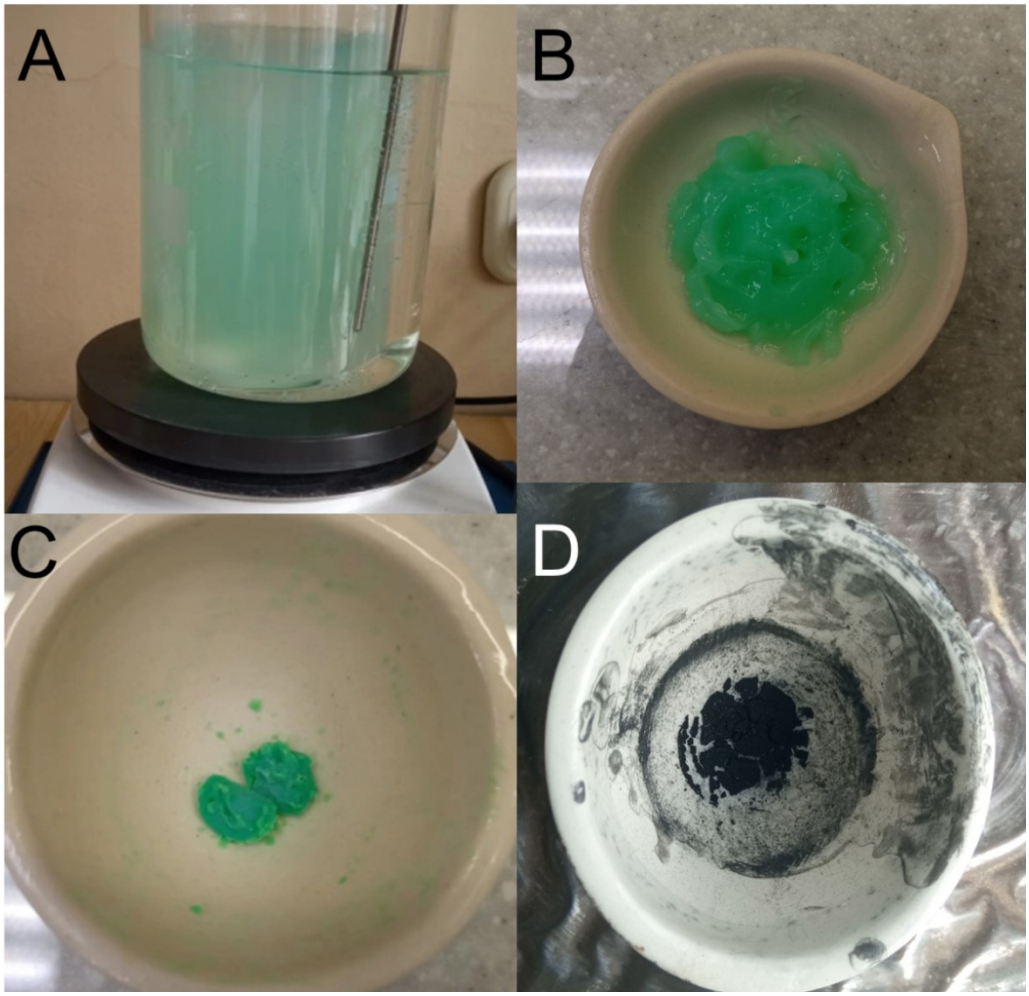

Fig. S2. Stages of synthesis of LNNS. (A) External appearance of LNNS formation upon addition of NaOH; (B) LNNS after precipitation, washing and concentration; (C) LNNS after overnight drying at +37 °C; (D) LNNS after calcination at +650 °C for 2 h.

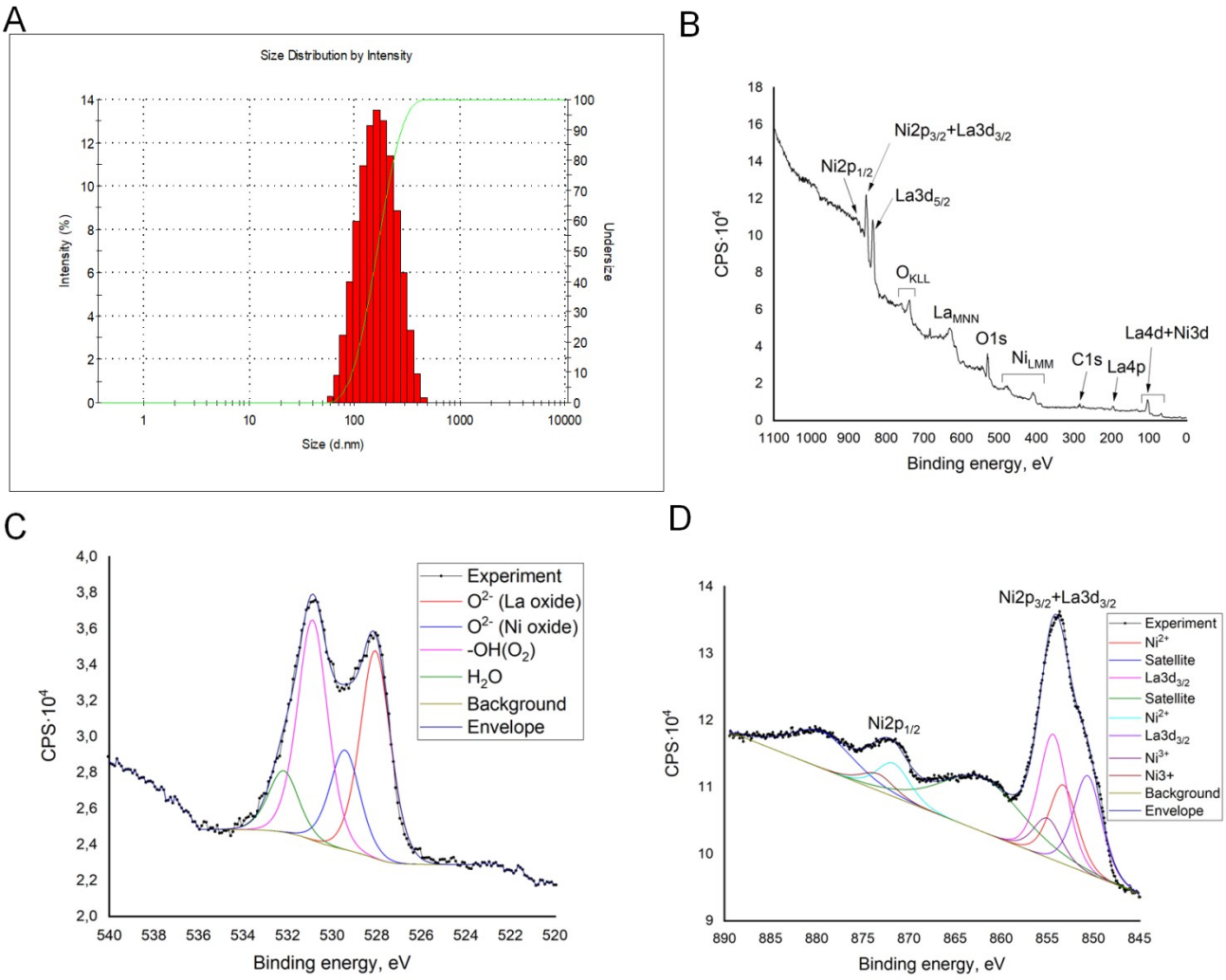

Fig. S3. (A) Size distribution of $LaNiO_3$ NS by intensity. (B) An overview spectra of the $LaNiO_3$ NS sample. (C) XPS signal of $LaNiO_3$ NS sample. (D) Deconvolution analysis of La3d and Ni2p3/2

Figures S4 and S6 show the results of energy dispersive microanalysis. For these studies, suspensions with $LaNiO_3$ (Fig. S4) and $LaNiO_3$@BSA/C6cc (Fig. S6) nanospheres were applied to an aluminum-magnesium alloy substrate and then dried in air. Scanning electron microscopy images were obtained on a Thermo Fisher Scientific Quattro S electron microscope at accelerating voltages in the range of 5 to 10 kV. Energy dispersive microanalysis was performed using an integrated EDAX Octane Elect Plus EDS System spectrometer.

Table S1. XRD analysis of LNNS

Rp: 5.88, Rwp: 7.85, Rexp: 3.97, global user-weigthed Chi2=3.92

Phase	Lattice parameter, Å	Weight, %
$LaNiO_3$ (R-3c)	5.4564, 5.4564, 13.1684	73 (72.87)
NiO (Fm-3m)	4.1881	13 (13.21)
La_2O_3 (Ia-3)	11.5274	3 (3.36)
La_2NiO_4 (I4/mmm)	5.2988, 12.9643	10 (10.30)
$LaNiO_3$ (R-3c)	5.4032, 12.4687	0 (0.27)

Table S2. Fitting results of La $3d_{3/2}$ and Ni 2p photoelectron spectra of $LaNiO_3$

Bond description	BE, eV	FWHM, eV	Concentration, %
$La3d_{3/2}$	850.15	3.88	11.41
Ni^{2+}	852.98	3.88	13.05
$La3d_{3/2}$	854.29	3.88	22.89
Ni^{3+}	854.68	3.88	6.52
Ni satellite	862.23	8.88	22.89
Ni^{2+}	871.38	4.51	6.52
Ni^{3+}	873.08	3.26	3.26
Satellite	879.12	8.31	13.25

The ratio of Ni^{2+}/Ni^{3+} is about 50%.

Table S3. Fitting results of O1s photoelectron spectra of $LaNiO_3$

Bond description	BE, eV	FWHM, eV	Concentration, %
O^{2-} (La oxide)	528.04	1.61	35.32
O^{2-} (Ni oxide)	529.33	1.61	16.11
-OH (O_2)	530.90	1.61	38.06
H_2O	532.10	1.61	10.50

A

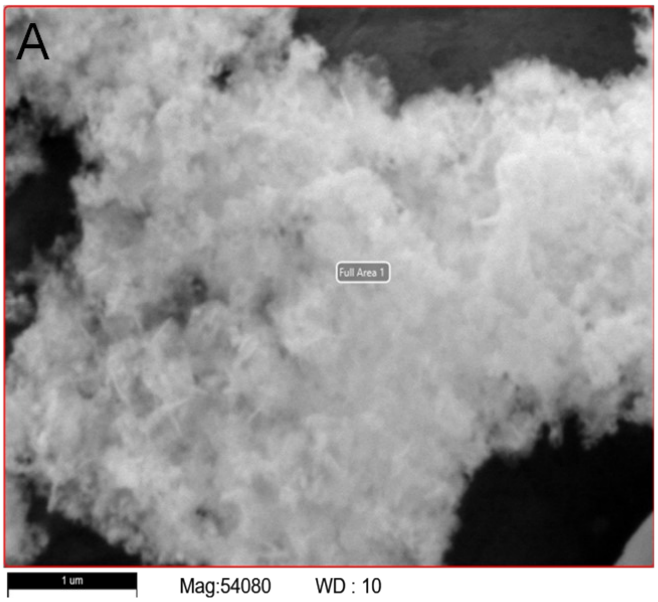

B

Element	Weight %	Atomic %	Error %
C	4.0	9.6	12.3
O	14.7	26.9	7.6
Mg	1.4	1.7	8.6
Al	48.0	52.1	5.0
Ni	10.3	5.1	7.1
La	21.6	4.5	9.8

C

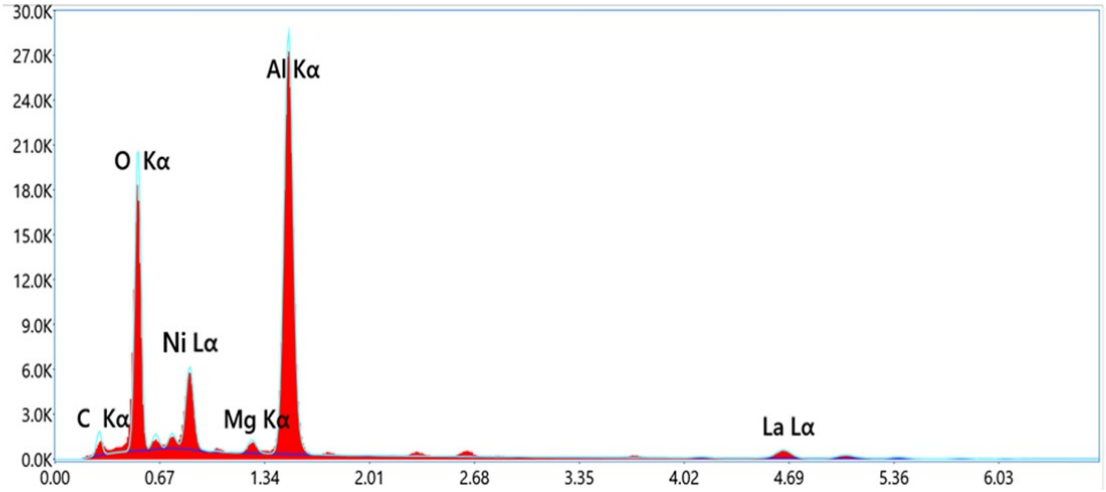

Fig. S4. (A) Signal collection area for the $LaNiO_3$ NS sample. (B) Elemental composition of the $LaNiO_3$ NS sample. (C) Energy dispersive X-ray spectrum for the $LaNiO_3$ NS sample.

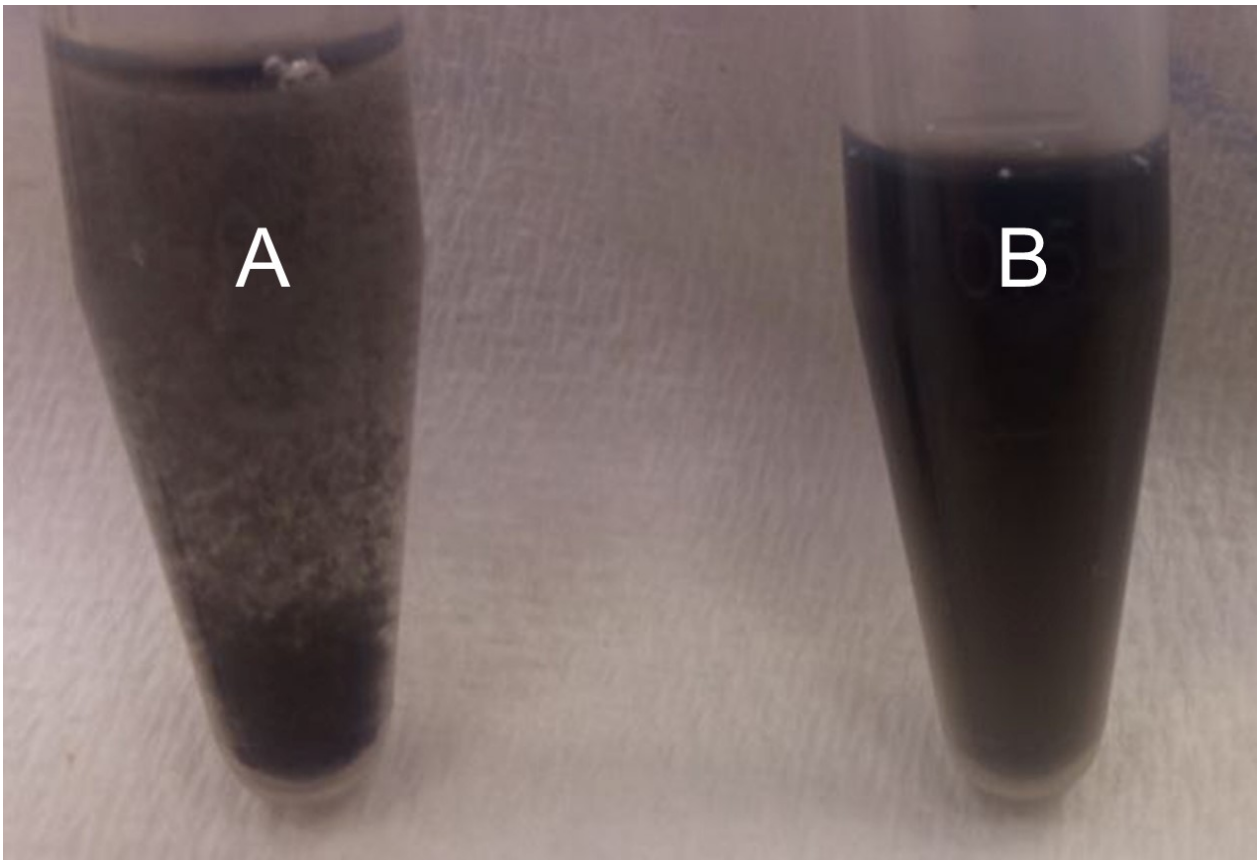

Fig. S5. (A) Aggregation process during fuctionalization stages of the LNNS; (B) Stabilization of the LNNS at the final stage of the diagnostic reagent produce.

A

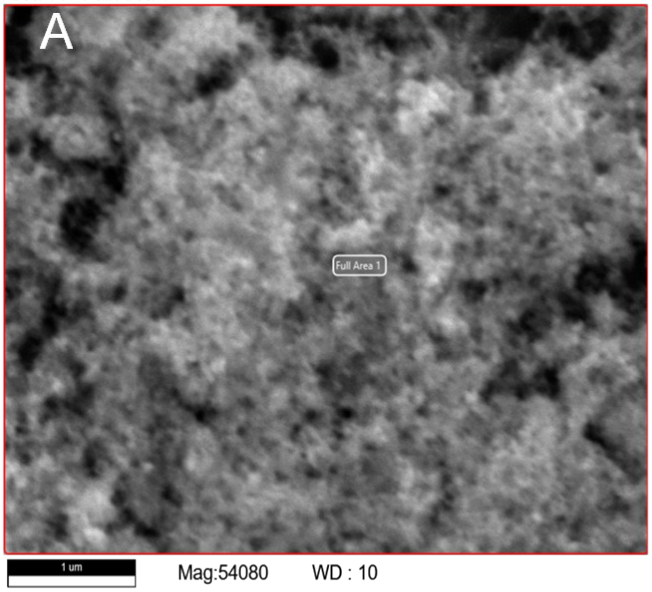

B

Element	Weight %	Atomic %	Error %
C	16.9	30.7	11.1
N	3.6	5.7	10.8
O	9.4	12.9	8.6
Mg	0.8	0.7	7.0
Al	56.8	46.0	3.8
P	2.5	1.7	6.5
Ni	3.5	1.3	7.2
La	6.4	1.0	9.0

C

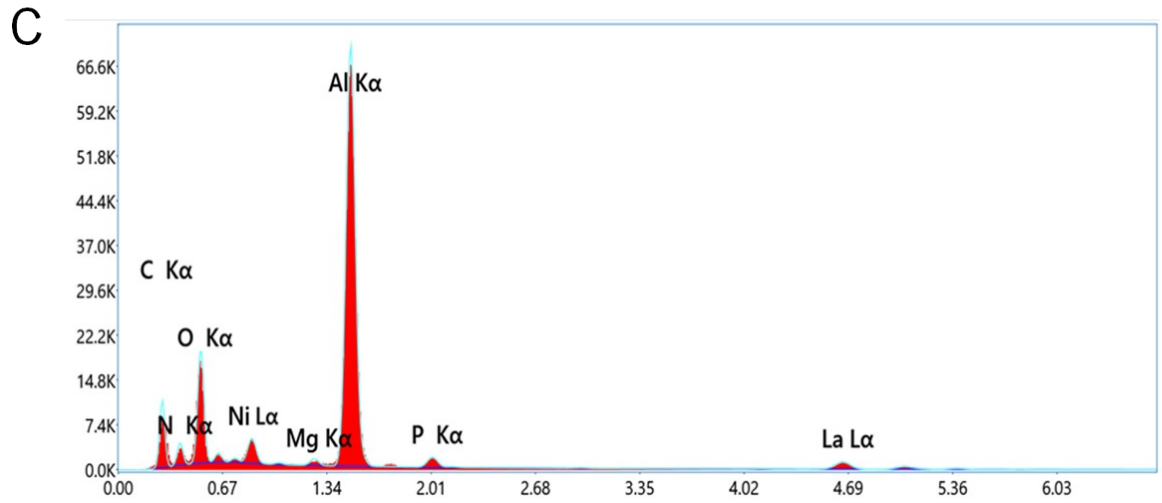

Fig. S6. (A) Signal collection area for the $LaNiO_3$@BSA/C6cc NS sample. (B) Elemental composition of the $LaNiO_3$@BSA/C6cc sample. (C) Energy dispersive X-ray spectrum for the $LaNiO_3$@BSA/C6cc NS sample.

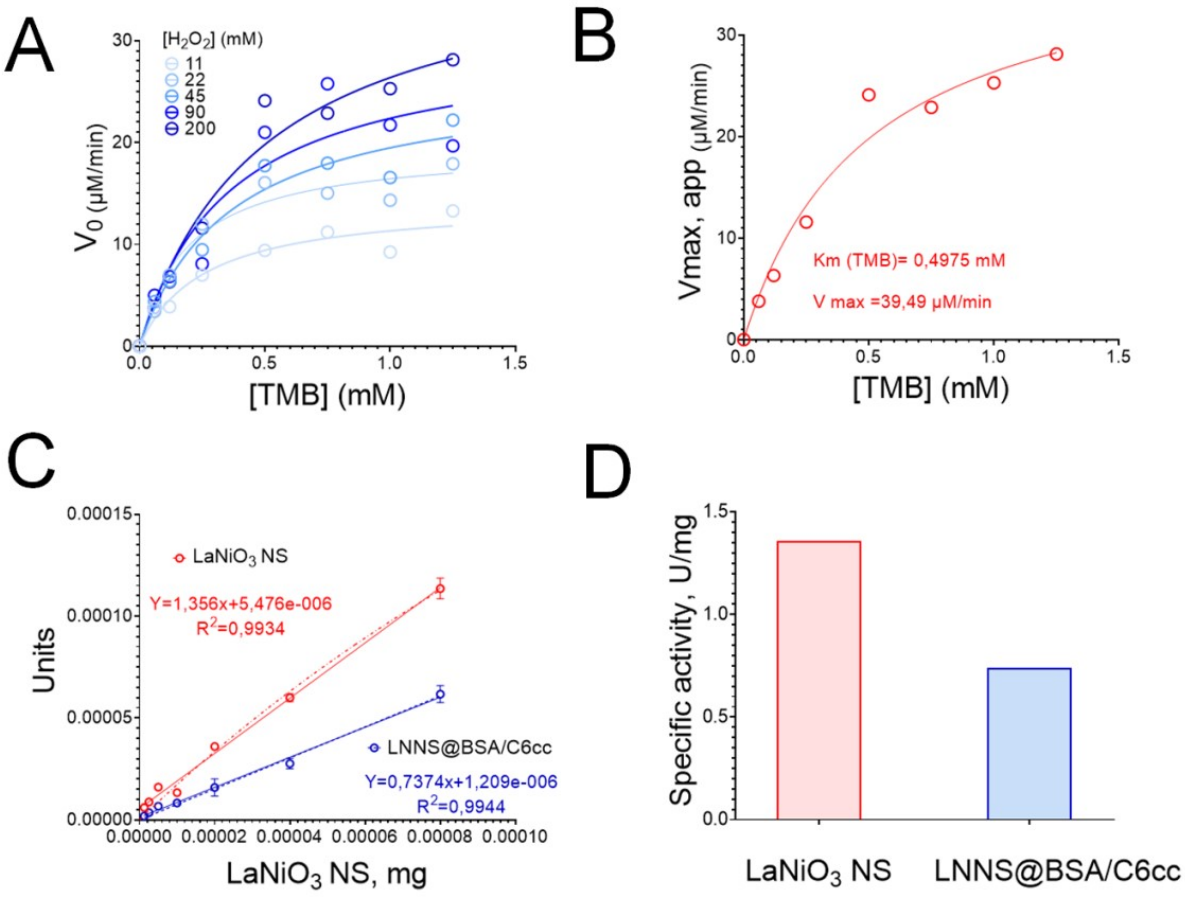

Fig. S7. (A,B) Kinetic study of $LaNiO_3$ NS using method based on the Michaelis–Menten equation. Plots of initial velocities (V_0) versus concentrations of (a) and its first fittings. Plots of apparent maximum velocities (Vmax,app) obtained from (A) versus concentrations of (B) H2O2 and (d) its second fittings to obtain the intrinsic maximum velocities (Vmax) and Michaelis constants (Km). (C) The determination of $LaNiO_3$ NS specific activities, n = 3, mean ± SD. (D) Specific activity of nanozymes before and after the functionalization.

Optimization of immunoassay parameters

C-reactive protein (CRP) is recognized as a key indicator of inflammation and can also be used to assess the risk of cardiovascular disease.[3] It was found that CRP levels below 1 mg/L indicate a potential risk of cardiovascular disease problems.[4] In the context of the assay design presented in this paper, and considering that serum samples require 1000-fold dilution, we focused on optimizing the assay conditions to generate a calibration curve with a steep slope of approximately 1 μg/L. This strategy will ensure accurate detection of CRP at concentration around 1 μg/L, will making the developed NLISA suitable for assessing cardiovascular risk.

Since the basal level of CRP in blood serum is 1 mg/L [3], finding human blood serum that does not contain CRP is problematic. Commercial mammalian blood sera can be used to optimize the conditions of the NLISA, but there are data on human CRP immunological cross-reactivity with CRP from almost all mammals for which commercially available sera exist (rabbit, bovine, horse, etc.). [5]

We examined the effect of sera from different mammalian species and used a blocking solution as a control. Four different commercial sera were diluted with a blocking solution to 0.1%. CRP was then diluted to 5 μg/L with 0.1% sera and LNNS-based NLISA was performed. It was shown that the use of 0.1% mammalian sera only slightly affects the analytical signal of the developed NLISA (Fig. S7A). In further studies, a blocking solution with the addition of 0.1% rabbit serum was used as a matrix for preparing calibration solutions of CRP (Fig. S7B).

As part of the optimization of the analysis procedure, the following parameters were optimized:

1) Concentration of the first (capturing) monoclonal antibodies (clone C2);
2) Dilution of the diagnostic reagent $LaNiO_3$@BSA/C6cc;
3) Composition of the blocking buffer.

The optimization results are presented in Fig. S7 B, C and D. It has been shown that the optimal parameters are:

1) Concentration of C2: 0.46 μg/ml;
2) $LaNiO_3$@BSA/C6cc dilution: 1:250;
3) The optimal blocking effect is achieved when using PBST with 1% BSA and 0.5% Casein as a blocking buffer.

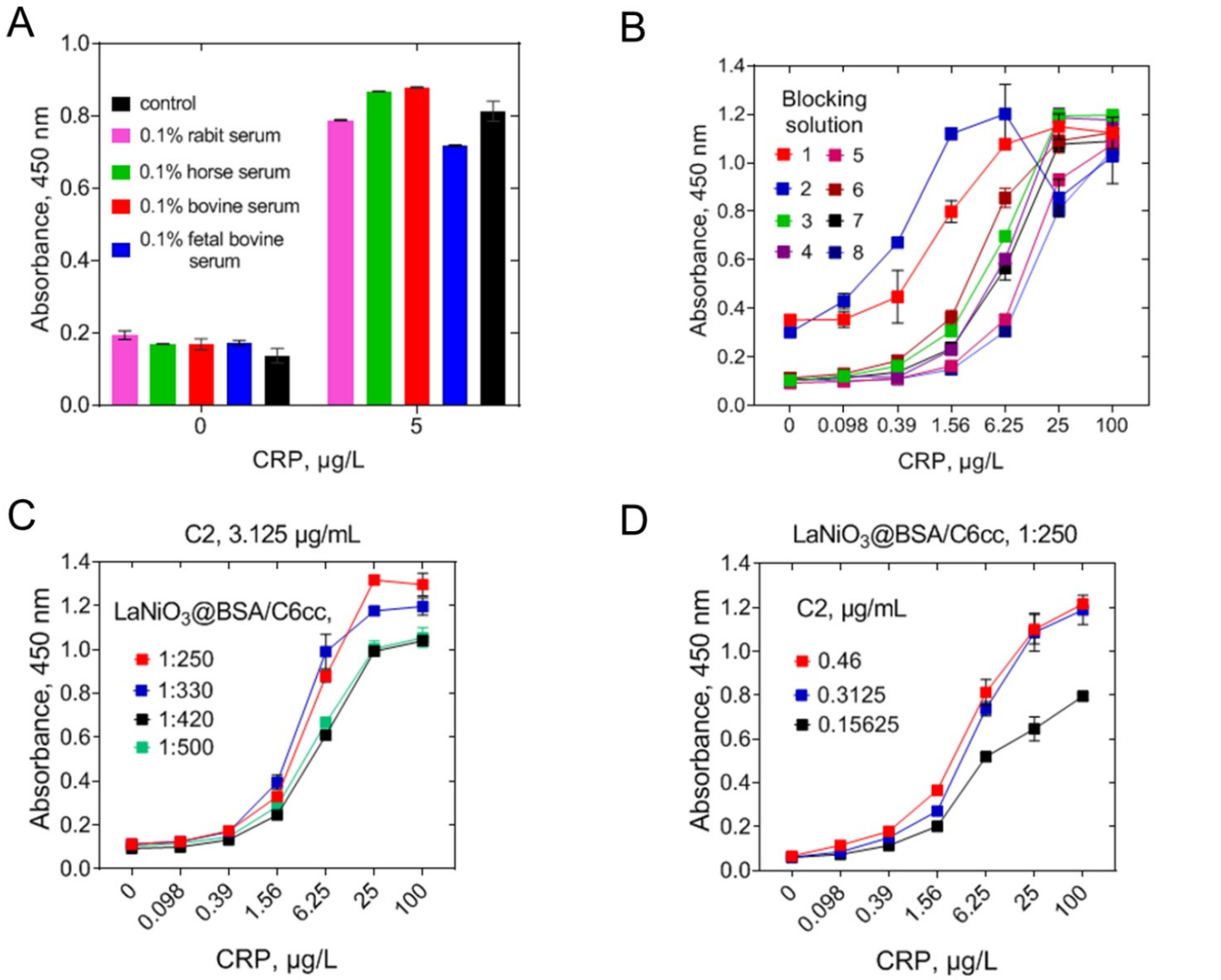

Fig. S8 Evaluation of optimal conditions for NLISA based on LaNiO3@BSA/C6cc. (A) Study of interference with mammalian blood sera. (B) Optimization of the composition of the blocking solution (1.PBST; 2.PBST + 1% BSA; 3.PBST + 0.5% Casein; 4.PBST + 1% Casein; 5.PBST + 2% Casein; 6.PBST + 1% BSA + 0.5% Casein; 7.PBST + 1% BSA + 1% Casein; 8.PBST + 1% BSA + 2% Casein). (C) Optimization of diagnostic reagent dilution (D) Optimization of capture monoclonal antibody concentration; Error bars indicate the standard deviation, n = 3

Table S4. Reproducibility of LNNS-based diagnostic reagent synthesis

Serum sample	CRP, mg/L (mean, n=3, Diagnostic reagent #1)	CRP, mg/L (mean, n=3, Diagnostic reagent #2)	CRP, mg/L (mean, n=3, Diagnostic reagent #3)	CRP, mg/L (mean)	Standard deviation	CV,%
1	6.71	5.93	8.19	6.94	0.94	13.49
2	0.29	0.49	0.44	0.41	0.08	20.22
3	5.43	4.94	6.45	5.60	0.63	11.24
4	4.34	4.05	4.30	4.23	0.13	3.12
5	1.46	1.46	1.44	1.45	0.01	0.81
6	0.96	1.01	0.98	0.98	0.02	2.15
7	2.33	2.14	2.05	2.17	0.12	5.36
8	0.86	0.85	0.89	0.87	0.01	1.70

Table S5. Validation of LNNS-based NLISA for CRP detection

Expected concentration, µg/L	Measured concentration, mg/L Mean, n=10	SD (n=10)	CV,%	Recovery index,%
0.098	0.08	0.045	55	62.12
0.195	0.18	0.04	23.5	92.6
0.39	0.42	0.057	13.4	108
0.78	0.81	0.07	8.6	104
1.56	1.595	0.13	8.35	102
3.125	2.67	0.07	2.59	85.36
6.25	6.52	1.05	16.1	104.3
12.5	12.48	1.026	8.22	99.86
25	16.5	2.14	13.32	64.3

Table S6. Spike-recovery test of LNNS-based NLISA for CRP sample in rabbit serum, diluted 1/1000 with blocking solution

Expected concentration, mg/L	Measured concentration, mg/L (n=6)	Recovery,%	SD (n=6)	CV,%
13	13.45	102.9	2.29	13.9
5	3.8	76.2	0.33	8
1	0.8	80.6	0.06	7.66
0.6	0.58	97.3	0.04	6.31
0.35	0.28	78.65	0.025	10.15

Table S7. LNNS-based NLISA precision

Serum sample	CRP, mg/L (mean, n=8)	Standard deviation	CV, %
1	0.6	0.06	11.2
2	12.1	1.821	14.5
3	5.1	0.87	15.4
4	11.1	1.78	16
5	1.4	0.12	8.35
6	1.44	0.18	12.56
7	3.5	0.49	14.05
8	1.3	0.23	17.26

Table S8. LNNS-based NLISA inter-day reproducibility

Serum sample	CRP, mg/L (mean, n=3, day 1)	CRP, mg/L (mean, n=3, day 2)	CRP, mg/L (mean, n=3, day 3)	CRP, mg/L (mean, n=3, day 4)	CRP, mg/L (mean, n=3, day 5)	CRP, mg/L (mean, n=5)	Standard deviation	CV. %
1	1.30	1.36	0.84	0.86	1.16	1.10	0.22	19.60
2	14.82	15.03	12.08	15.40	13.24	14.11	1.26	8.92
3	1.27	1.09	0.75	1.00	0.98	1.02	0.171	16.76
4	12.51	10.90	10.33	9.63	10.23	10.72	0.98	9.16
5	9.34	7.86	8.87	11.31	8.05	9.09	1.24	13.60
6	3.06	2.64	2.60	2.84	2.59	2.75	0.18	6.63
7	16.81	15.76	17.18	15.58	12.98	15.66	1.47	9.40
8	2.37	1.91	1.85	2.03	1.94	2.02	0.18	9.03
9	3.72	4.13	4.09	4.60	4.21	4.15	0.28	6.76
10	3.20	1.95	1.97	2.54	2.15	2.36	0.47	19.88

Table S9. Concentration of CRP in serum samples measured by LNNS-based NLISA and immunofluorescent assay, mg/L

Serum sample	NLISA (n=3)	Immunofluorescent assay (n=3)	Average	% Difference
1	0.35	0.4	0.38	-13.33
2	1.06	1.1	1.08	-3.7
3	17.83	18	17.9	-0.95
4	1.04	1.4	1.22	-29.5
5	0.45	0.5	0.475	-10.53
6	12.5	14.5	13.5	-14.81
7	11.31	12	11.7	-5.92
8	20.04	19.9	19.97	0.7
9	105.73	104.9	105.3	0.79
10	130.88	117.4	124.1	10.86
11	5.41	6.1	5.76	-11.99
12	3.2	2.5	2.85	24.56

References

1 P. Li, C. Tian, W. Yang, W. Zhao and Z. Lü, *Front. Mater. Sci.*, 2019, **13**, 277–287.
2 Y. Qiu, R. Gao, W. Yang, L. Huang, Q. Mao, J. Yang, L. Sun, Z. Hu and X. Liu, *Chem. Mater.*, 2020, **32**, 1864–1875.
3 I. Kushner, *Front. Immunol.*, 2023, **14**, 1150103.
4 T. A. Pearson, G. A. Mensah, R. W. Alexander, J. L. Anderson, R. O. Cannon, M. Criqui, Y. Y. Fadl, S. P. Fortmann, Y. Hong, G. L. Myers, N. Rifai, S. C. Smith, K. Taubert, R. P. Tracy and F. Vinicor, *Circulation*, 2003, **107**, 499–511.
5 A. Pathak and A. Agrawal, *Front. Immunol.*, 2019, **10**, 943.